Materials Today Bio 20 (2023) 100662

Contents lists available at ScienceDirect

Materials Today Bio

journal homepage: www.journals.elsevier.com/materials-today-bio

A scalable culture system incorporating microcarrier for specialised mesenchymal stem cells from human embryonic stem cells

Tingting Gao [a,d,1], Xiyuan Zhao [a,c,d,1], Jie Hao [b,c,d,1], Yao Tian [a,d], Huike Ma [e], Wenjing Liu [c], Bin An [a], Faguo Sun [a,d], Shasha Liu [a,d], Baojie Guo [a,d], Shuaishuai Niu [b,c], Zhongwen Li [a,c], Chenxin Wang [a,c], Yukai Wang [a,c,d], Guihai Feng [a,c,d], Liu Wang [a,c,d], Wei Li [a,c,d], Jun Wu [a,c,****], Meijin Guo [e,***], Qi Zhou [a,c,d,**], Qi Gu [a,c,d,*]

[a] State Key Laboratory of Stem Cell and Reproductive Biology, State Key Laboratory of Membrane Biology, Institute of Zoology, Chinese Academy of Sciences, Beijing 100101, China
[b] National Stem Cell Resource Center, Institute of Zoology, Chinese Academy of Sciences, Beijing 100101, China
[c] Beijing Institute for Stem Cell and Regenerative Medicine, Beijing 100101, China
[d] University of Chinese Academy of Sciences, Beijing 100049, China
[e] State Key Laboratory of Bioreactor Engineering, East China University of Science and Technology, Shanghai 200237, China

ARTICLE INFO

Keywords:
Mesenchymal stem cells
Human embryonic stem cells
Microcarrier
Bioreactor
Culture system

ABSTRACT

Mesenchymal stromal cells (MSCs) derived from human embryonic stem cells (hESCs) are a desirable cell source for cell therapy owing to their capacity to be produced stably and homogeneously in large quantities. However, a scalable culture system for hPSC-derived MSCs is urgently needed to meet the cell quantity and quality requirements of practical clinical applications. In this study, we developed a new microcarrier with hyaluronic acid (HA) as the core material, which allowed scalable serum-free suspension culture of hESC-derived MSCs (IMRCs). We used optimal microcarriers with a coating collagen concentration of 100 μg/mL or concave-structured surface (cHAMCs) for IMRC amplification in a stirred bioreactor, expanding IMRCs within six days with the highest yield of over one million cells per milliliter. In addition, the harvested cells exhibited high viability, immunomodulatory and regenerative therapeutic promise comparable to monolayer cultured MSCs while showing more increased secretion of extracellular matrix (ECM), particularly collagen-related proteins. In summary, we have established a scalable culture system for hESC-MSCs, providing novel approaches for future cell therapies.

1. Introduction

Mesenchymal stromal cells (MSCs) and extracellular vesicles derived from MSCs have become important components in many clinical trials. The amount of MSCs needed per patient ranges from tens of millions to billions per kilogram of body weight, depending on the disease being treated [1–3]. Human pluripotent stem cells (hPSCs) such as human embryonic stem cells (hESCs) and human induced pluripotent stem cells (hiPSCs), have unlimited proliferation and differentiation potential, making them reliable sources of functional cells for large-scale expansion [4–6]. MSCs differentiated from hPSCs have been proven feasible, exhibiting typical MSC properties both in vitro and in vivo, such as multi-lineage differentiation ability and immunomodulatory effects. This makes them a promising strategy for future cell-based therapies [7,8]. In previous studies, clinical-grade hESCs were differentiated to MSC-like populations with the unique abilities to modulate immunity and regulate

* Corresponding author. State Key Laboratory of Stem Cell and Reproductive Biology, State Key Laboratory of Membrane Biology, Institute of Zoology, Chinese Academy of Sciences, Beijing 100101, China.
** Corresponding author. State Key Laboratory of Stem Cell and Reproductive Biology, State Key Laboratory of Membrane Biology, Institute of Zoology, Chinese Academy of Sciences, Beijing 100101, China.
*** Corresponding author. State Key Laboratory of Bioreactor Engineering, East China University of Science and Technology, Shanghai 200237, China
**** Corresponding author. State Key Laboratory of Stem Cell and Reproductive Biology, State Key Laboratory of Membrane Biology, Institute of Zoology, Chinese Academy of Sciences, Beijing 100101, China.
E-mail addresses: wuxf@ioz.ac.cn (J. Wu), guo_mj@ecust.edu.cn (M. Guo), qzhou@ioz.ac.cn (Q. Zhou), qgu@ioz.ac.cn (Q. Gu).
[1] Three authors contributed equally to this work.

https://doi.org/10.1016/j.mtbio.2023.100662
Received 7 March 2023; Received in revised form 20 April 2023; Accepted 5 May 2023
Available online 5 May 2023
2590-0064/© 2023 Published by Elsevier Ltd. This is an open access article under the CC BY-NC-ND license (http://creativecommons.org/licenses/by-nc-nd/4.0/).

extracellular matrix production, also known as immunity- and matrix-regulatory cells (IMRCs) [9]. hESC-derived IMRCs have been tested in preclinical studies for therapeutic effects in various diseases [9–11] and have also shown encouraging results in clinical trials for diseases such as COVID-19-associated acute lung injury (ALI) and pulmonary fibrosis, with good results [12,13]. With the increasing application of hPSC-derived MSCs, the large-scale preparation of cells that meet the quality requirements needs to be addressed. Although two-dimensional (2D) culture has the advantage of being simple, several issues, such as complex processes and high cost hinder its usefulness in the systematic development of mass production [14–16].

Bioreactor-based three-dimensional (3D) culture technology creates a specialised microenvironment for producing stem cells. It enables the real-time control of culture parameters to meet the growing demand for cell production [17–19]. Stirred bioreactors using microcarriers offer a high-density suspension culture for large-scale MSC production with sufficient surface area for cell attachment and expansion [20,21]. Since the earliest reported particle, positively charged DEAE-Sephadex beads [22], microcarrier technology has rapidly developed for large-scale culture of various cell types [2]. Commercial microcarriers exhibit different properties that affect cell growth, mainly including surface characteristics, core materials, size and curvature [2,23]. The selection of core materials for microcarriers is crucial to their performance, and commonly used materials include polystyrene, gelatin, polyvinyl alcohol, dextran, glass or other components [24,25]. Notably, microcarriers with the same biological coating but different core materials can yield in distinct outcomes in MSC production. For instance, Cytodex-3 and SoloHill Collagen microcarriers exhibit different performance despite having an identical biological coating [24]. Therefore, the screening of more suitable matrix materials is an essential strategy to optimise microcarrier properties.

Hyaluronic acid (HA) is a natural glycosaminoglycan (GAG) polysaccharide widely distributed in vertebrates that is challenging to apply in the microcarrier field due to its long linear polymer chain and easy solubility in water [26,27]. HA-related hydrogels offer many advantages, such as chemical modification into various physical forms, which can provide a niche for MSCs while preserving their cellular properties [28–31]. Previous studies have produced HA-based hydrogel microspheres and acrylate HA microcarriers [32,33], but the potential of HA microcarriers for stem cell expansion in scalable bioreactors has yet to be explored.

This study evaluated whether microcarriers made with HA as the core material were suitable for IMRC suspension culture using scalable bioreactor technology in serum-free culture and while maintaining their characteristics and immunomodulatory capacity. IMRCs were expanded on HA microcarriers (HAMCs) and concave-structured microcarriers (cHAMCs) in stirred bioreactors, resulting in excellent cell properties and immunomodulatory potential.

2. Materials and methods

2.1. Materials

Hyaluronic acid (average molecular weight of 90–100 kDa) was obtained from DuoXi (Shanghai, China); *N*-hydroxy succinimide (NHS) was purchased from Sigma, while a 1-(3-dimethylaminopropyl)-3-ethyl carbodiimide hydrochloride (EDC), NH_4HCO_3, liquid paraffin, span 80, and other chemically pure reagents were purchased from Aladdin (Shanghai, China). Collagen type I was purchased from Advanced Biomatrix. Commercial microcarriers m-Dev45 (Coring), Cytodex-3 (GE Healthcare), SoloHill (Sigma) and Cultispher (Thermo Scientific) were purchased from their respective distributors.

2.2. HA microcarriers preparation

To prepare HA microcarriers (HAMCs), HA powder (500 mg) was dissolved in 10 mL of deionised water at room temperature. EDC (0.766 mg) and NHS (0.288 mg) powders were added to the HA solution, and the mixture was stirred for 5 min to obtain a crosslinked solution at room temperature. The solution was added dropwise to 80 mL of liquid paraffin containing 0.25 mL of span 80 under stirring at 700 rpm and 40 °C to form a W/O emulsion. After stirring for 16 h at 25 °C, HA-NHS ester spheres were obtained. To get concave-structured HA microcarriers (cHAMCs), 0.3 wt% ammonium bicarbonate was added to the oil phase during preparation. The resulting microspheres were collected by centrifugation (4 °C, 7000 rpm, 5 min) and washed five times with 75% ethanol and then washed 5 times with double-distilled water (DDW) by centrifugation. The microspheres were then coated with collagen by placing them in 200 mL of the aqueous solution containing 20 mg of collagen at 4 °C for 12 h. The crosslinked microspheres were washed 5 times with DDW by centrifugation (4 °C), freeze-dried, and sterilised with ethylene oxide gas.

2.3. Fourier transform infrared (FTIR) spectroscopy analysis of HAMC

The chemical composition of the microcarrier blends and various substances, including HA powder, HAMC, HA-NHS ester, and NHS, were analysed using Fourier transform infrared (FTIR) spectroscopy. The microcarriers freeze-dried after being frozen at −80 °C and analysed using attenuated total reflectance spectra (ATR-FTIR) were obtained from an infrared spectrometer (Nicolet iS50, Thermo Scientific, USA). A total of 64 scans were accumulated in the 4000 to 400 cm^{-1} range at a resolution of 4 cm^{-1}. The background FTIR spectra for different samples were recorded and subtracted from the sample spectrum to obtain the final spectra.

2.4. Atomic force microscopy (AFM)-based local stiffness measurement

To allow the measurement of the local modulus for microcarriers in AFM, the microcarriers were glued to the glass sheet for AFM microscopy. A small bead (radius, 15 μm) was immobilised at the terminus of the AFM tip prior to testing. During the test, the tip was controlled to approach the debris with a speed of 25 μm/s until the bead reached the debris and a force over 5 nN was generated between the bead and the debris. The tip was controlled to detach from the microcarriers to finish a single test for local stiffness. The force-displacement curve was recorded during the whole process, from which the local Young's modulus could be calculated. This experimental design gave us over 60 stiffness values for each group in every experiment, resulting in over 180 data points for each group in total [34].

2.5. hESC-derived MSCs differentiation and monolayer culture

hESC-derived MSCs (immunity- and matrix-regulatory cells, IMRCs) have been previously generated from clinical hESCs and induced to migrate out from human embryoid bodies (hEBs) in serum-free reagents following the previous protocol [9]. IMRCs (passage 3, P3) were obtained and seeded into plates or flasks at 1×10^4 cells/cm^2. Cells were expanded in "IMRC Medium" containing α-MEM (Gibco), 5% KOSR, 1% Ultroser G (Pall corporation), 1 × L-glutamine, 1 × NEAA, 5 ng/mL bFGF and 5 ng/mL TGF-β (Peprotech) and refreshed every 2 days. Cells were dissociated or passaged by using Tryple (Gibco) upon reaching 70%–80% confluence in conditioned medium.

2.6. Cell expansion on microcarriers under static conditions

Different microcarriers and cells were placed into plates with ultralow attachment surfaces (Corning) in a working volume of 10 mL. The microcarriers were washed with PBS and cells were digested using 5 mL of Tryple after 7 days. Cell number and viability were tested using Trypan Blue by Countstar software (Ruiyu BioTech, China).

2.7. IMRC suspension culture in stirred bioreactors

According to the instructions, the bioreactor was used in the suspension culture of IMRCs (DASbox Mini bioreactor system, Eppendorf). The bioreactor consists of 250 mL glass vessels, each equipped with a 3-blade impeller (30° pitch), dissolved oxygen (DO) and potential of hydrogen (pH) probes, and temperature and gassing control modules, enabling the online monitoring of cell culture conditions. DO and pH were calibrated before each culture.

For IMRC suspension culture, IMRCs were seeded onto 0.1 g of Cytodex-3 or HAMC at a density of 1.0×10^5 cells/mL in bioreactors containing 100 mL of IMRC medium. Cells were cultivated at 37 °C with constant headspace gassing and stirring. The DO (40%) and pH (7.2) were controlled by gassing. Starting from day 2, a bioreactor refreshed half of the IMRC medium daily. To assess cell expansion in the bioreactor, 1 mL of suspension was sampled from the Port (sampling) every day ($n = 3$). The supernatant was removed after precipitation, and microcarriers were exposed to Tryple (Gibco) at 37 °C until digested into single cells. Cell density were then tested. After 7 days, IMRCs were digested and separated from microcarriers using a 40 μm cell strainer. The attachment efficiency of IMRCs on different microcarriers was calculated as the number of IMRCs attached to microcarriers at 3 or 24 h divided by the total number of cells inoculated at 0 h.

2.8. Size analysis of cells and microcarriers

The size of IMRCs harvested from monolayers or microcarriers was determined by microscopy and ImageJ software (National Institutes of Health). The cells were transferred into the chambers of a cell counter and photographed by microscopy. Subsequently, the cell diameter of more than 900 cells per group was measured using ImageJ. Normal distribution curves were fitted to the cell diameter data to analyse the cell size distribution characteristics by Gaussian distribution. Finally, ImageJ was used to determine the diameter of the randomly selected microcarriers ($n = 340$).

2.9. Growth curves

IMRCs derived from monolayers or microcarriers were seeded at 1.2×10^3 cells per well in 96-well plates (Corning) in triplicate and cultured for 7 days. Cell Counting Kit-8 (CCK-8; Thermo Fisher Scientific) was used to investigate cell proliferation. After 1, 3, and 7 days, the medium was replaced by CCK-8 solution, incubated for 2 h and tested at 450 nm.

2.10. Karyotype analysis

IMRCs were harvested from monolayers or HAMCs after 6 days. A total of 1×10^6 cells were analysed by G-binding. Karyotyping was executed at CapitalBio Technology (Beijing, China).

2.11. Senescence detection

IMRCs harvested from monolayers or microcarriers were seeded into 6-well plates at 1×10^4 cells/cm^2. IMRCs were fixed, and cell senescence was detected using a β-galactosidase (β-gal) staining kit (Solarbio) on day 3. Then, cells positive for β-gal activity were observed under a microscope.

2.12. Flow cytometry analysis

IMRCs were digested into single cells and blocked with 2% bovine serum albumin (BSA; Sigma-Aldrich) for 30 min. Then, cells were stained by incubation with PE-labeled anti-human CD11b (Biolegend), CD19 (BD Biosciences), CD29 (Biolegend), CD34 (BD Biosciences), CD73 (BD Biosciences), CD105 (Biolegend), CD90 (eBioscience), FITC-labeled anti-human HLA-ABC (BD Biosciences), and PE- or FITC-labeled isotype-controlled antibodies (BD Biosciences). After 30 min of incubation, the cells were washed and resuspended in PBS, and the expression of cell-specific markers was analysed by MoFlo (Beckman, Brea, CA, USA).

2.13. Interferon-gamma (IFN-γ) stimulation assay

IMRCs derived from monolayer culture or HAMC expansion were harvested and seeded at 3×10^5 cells/well in 6-well plates. After culturing for 24 h, the medium was replaced with a medium containing different concentrations of IFN-γ (0, 50 and 100 ng/mL) (R&D Systems) and cultivated for 24 h. After IFN-γ stimulation, cells were harvested for qPCR.

2.14. qPCR

The total mRNA from IMRCs was extracted by an RNAprep Pure Cell/Bacteria Kit (TIANGEN, China). Complementary DNA (cDNA) was synthesised by RNA reverse transcription using a PrimeScript™ First-Strand cDNA Synthesis Kit (TaKaRa, Japan). qPCR was performed and analysed by SYBR Green Real-Time PCR Master Mix Plus (Toyobo) using a LightCyoler®480 system (Roche, USA). *GAPDH* was used for internal normalisation. The following primers were used for real-time PCR:

IDO1-forward GCCAGCTTCGAGAAAGAGTTG.
IDO1-reverse ATCCCAGAACTAGACGTGCAA.
GAPDH-forward CTCTGCTCCTCCTGTTCGAC.
GAPDH-reverse CGACCAAATCCGTTGACTCC.

2.15. IMRC inhibition of PBMC proliferation

Human peripheral blood mononuclear cells (PBMCs) were thawed and resuspended in RPMI 1640 medium supplemented with 10% FBS and 1% penicillin-streptomycin, then seeded at 1×10^5 cells/well into 96-well plates. CD3/CD28 beads and IL-2 stimulated the activated PBMCs. IMRCs were harvested from either monolayers or HAMCs were immediately added into the above-activated PBMCs at various densities (5×10^4, 5×10^3, 1×10^3, or 0 cells per well). PBMCs without IMRCs at the same density served as a reference control ($n = 5$). On the fourth day of culture, PBMC proliferation was detected by CCK-8 assay.

2.16. Multiplex cytokine analysis

Supernatants of PBMCs, activated PBMCs and IMRCs/activated PBMCs were collected after 4 days of culture and stored after light centrifugation. The thawed supernatants were analysed by 48-plex Bio-Plex Pro Human Cytokine Assay (Bio-Rad, Hercules, CA, USA) according to the manufacturer's instructions. The cytokines are CTACK, Eotaxin (CCL11), FGF basic, granulocyte-colony stimulating factor (G-CSF), granulocyte-macrophage colony-stimulating factor (GM-CSF), GRO-α, HGF, IFN-α2, IFN-γ, interleukin-1α (IL-1α), IL-1β, IL-1RA, β-NGF, MIP-1α (CCL3), MIP-1β (CCL4), MIG, MIF, M-CSF, LIF, MCP-3, MCP1 (CCL2), IP10 (CXCL10), IL-8 (CXCL8), RANTES (CCL5), IL-18, IL-17α, IL-16, IL-2, IL-2Rα, PDGFB, SCF, SCGF-β, SDF-1α, tumor necrosis factor alpha (TNF-α), TNF-β, TRAIL, VEGF, IL-3, IL-4, IL-5, IL-6, IL-7, IL-9, IL-10, IL-12 (p70), IL-12 (p40), IL-13, and IL-15.

2.17. Live/dead test

The IMRC-laden microcarriers were transferred to a 96-well plate, and the supernatant was aspirated after precipitation and washed with PBS. Then, 200 μL of Live/dead dye solution was added and incubated away from light at room temperature. The Live/dead staining solution was obtained by diluting calcein AM and ethidium homodimer-1 (EthD-1) with PBS according to the manufacturer's instructions (Thermo Fisher Scientific). After 30 min, the supernatant was aspirated, washed with PBS, and imaged with an inverted fluorescence microscope (Zeiss, Germany).

2.18. Glucose and lactate analysis

During the suspension culture of IMRCs, 1 mL of cell culture supernatant was collected before and after changing the IMRC medium every day and analysed using SBA-Biosensing Analyser (Yanhe Biological, China) for glucose and lactate concentration in medium (n = 3 per group, per time point).

2.19. Characterisation of IMRC-laden microcarriers and HAMC

Scanning electron microscopy (SEM) imaging IMRC-laden microcarriers were fixed with 2.5% glutaraldehyde overnight at 4 °C, precipitated and washed with PBS 3 times and serially dehydrated with 30%, 50%, 75%, 85%, and 100% ethanol. Samples were then CO_2 critical point dried and gold-coated before SEM (Hi-tachi, Japan) imaging. An energy dispersive spectrometer (EDS) was used to analyse the HAMC elementally. Corresponding electrokinetic measurements (zeta potential) of the HA-NHS ester and HAMC surfaces was tracked using a zeta potential analyser (NanoBrook 90Plus PALS, USA). In order to facilitate the process of contact angle measurement, the materials for preparing microcarriers were cut into rectangular shapes, and HA-NHS ester and HA-COL were evaluated using a Kruss Drop Shape Analyser (Germany).

2.20. Trilineage differentiation

Osteogenic, adipogenic, and chondrogenic differentiation were evaluated according to the manufacturer's instructions for the human mesenchymal stem cell functional identification kit (R&D systems), as previously described [9]. Briefly, for osteogenic differentiation and adipogenic differentiation, cells were seeded in 12-well plates, and when cells reached 50%–70% and 100% confluency, the medium was replaced with osteogenic differentiation medium or adipogenic differentiation medium and then cultured for 21 days. After 21 days of differentiation, cells were fixed and subjected to detection of osteogenic differentiation by either osteocalcin immunofluorescence or Alizarin Red S staining (Sigma-Aldrich). Adipogenic differentiation was assessed by either FABP-4 immunofluorescence or Oil red O staining (Sigma-Aldrich). For chondrogenic differentiation, 2.5×10^5 cells were placed in a chondrogenic differentiation medium, centrifuged for 5 min at 200 × *g* in a 15 mL centrifuge tube (Corning), and then cultured for 21 days. Chondrogenic pellets were fixed, paraffin-embedded, sectioned, and then subjected to detection of chondrogenic differentiation was detected by immunofluorescence (Aggrecan) or Alcian Blue (Sigma-Aldrich) staining. To detect trilineage differentiation in situ of cell-laden microcarriers, the IMRC-laden microcarriers from the bioreactor were transferred to 15 mL centrifuge tubes, and the trilineage differentiation medium was added and then cultured for 21 days after replacement of the supernatants.

2.21. Immunofluorescence of IMRC-laden microcarriers

We collected IMRC-laden microcarriers from the bioreactor and fixed them with 4% paraformaldehyde (PFA) at 4 °C overnight in 8-well plates. After washing the samples in PBS, we blocked them with 2% BSA for 1 h at room temperature. Then, the samples were incubated overnight with phalloidin (Invitrogen) at a dilution of 1:200 and vinculin (Invitrogen) at a dilution of 1:200 in 2% BSA at 4 °C. Following this, the samples were washed three times with PBS and then stained with fluorescein (Cy3) donkey anti-rabbit IgG (H + L) (Jackson ImmunoResearch) secondary antibodies at a dilution of 1:200 in 2% BSA for 1 h in the dark at room temperature. DAPI (Beyotime) at a dilution of 1:1000 was used to stain the samples for 5 min after washing. Finally, we captured images using a confocal laser scanning microscope (Zeiss, Germany).

2.22. RNA-seq library preparation and bioinformatic analysis

Total RNA from IMRCs harvested from monolayers or microcarriers was extracted using TRIzol reagent (Invitrogen). RNA-seq libraries were built for Illumina® using the NEBNext®Ultra™ RNA Library Prep Kit. Sequencing was performed on an Illumina HiSeq X-Ten sequencer with a 150 bp paired-end sequencing reaction. After the sequencing data were filtered, they were mapped to the reference genome hg38 using STAR. Gene expression levels were estimated by counting sequencing sequences (reads) mapped to genomic regions or exon regions and FPKM (Fragments per Kilobase per Million Mapped Fragments) [35]. DESeq2 was used for differentially expressed gene (DEG) analysis, and the screening criteria for DEGs in this project were $|\log2\text{-fold change}| \geq 1$ and P value < 0.05. Principal component analysis (PCA) of RNA-seq data of cell samples was performed using the prcomp function in R. Heatmap, and Volcano map analyses were performed with the pheatmap and ggscatter functions in R. The Pearson correlation coefficient was calculated by cor.test in R. Gene Ontology and KEGG pathway analyses for DEGs were performed by the clusterProfiler package.

2.23. Statistics

We performed statistical analysis using GraphPad Prism 9.0 software (GraphPad Software, San Diego, CA, USA). The results were presented as mean ± standard deviation (Mean ± S.D). Statistical differences among groups were assessed using ordinary one-way ANOVA or unpaired *t*-test. A p-value of less than 0.05 was considered statistically significant. The legend is as follows: ns = not significant, *p < 0.05; **p < 0.01; ***p < 0.001; ****p < 0.0001.

3. Results

3.1. Design and production of HA microcarriers

Fabricating HA-based microcarriers with pure HA remains a challenge due to slow hardening rate and the instability of unmodified HA hydrogels, making them ineffective microcarrier fabrication [36]. To address this issue, we activated the carboxylic acid groups on the hyaluronic acid molecule chain using EDC and NHS to produce HA-NHS ester [37]. The HA-NHS ester was then crosslinked with free amino groups of type I collagen, forming stable amide bonds and producing HAMCs. Different sized HAMCs were obtained using stainless steel wire mesh sieves with varying pore sizes (Fig. 1A). HAMCs had a smooth surface and an average particle size of 150 μm in wet condition (Fig. 1B). Elemental analysis via STEM-based line scanning revealed uniform distribution of C, N, O, and Na in the microcarrier elements, confirming the formation of coordination structures (Fig. 1D). FTIR was used to assess the structural changes of HA, HA-NHS ester, HAMC and NHS. A peak at 3300 cm^{-1} confirmed –OH stretching vibration in Fig. 1C. The formation of HA-NHS ester was evident from a new band at 1740 cm^{-1} and disappearance of the NHS absorption band at 3110 cm^{-1}. HAMC showed characteristic peaks at 1645 cm^{-1} and 1550 cm^{-1}, corresponding to collagen amide I and II, respectively. COO^- stretching and the amide II band were assigned to the peaks at ~1607 cm^{-1} and ~1560 cm^{-1}, respectively, in HA. In addition, the determination of surface charge on the microcarrier was shown in Fig. S1, where the zeta potential of HA-NHS ester without collagen modification was approximately −0.69 mV, and that of HAMC was approximately −0.17 mV. This indicates that the core material HA-NHS ester has weak electronegativity, and the surface electronegativity of the microcarrier is reduced after collagen modification. We also performed contact angle tests on HA-NHS ester and HA-COL, and the results were shown in Fig. S2. The water contact angles of HA-NHS ester and HA-COL were 33° (Fig. S2A) and 70° (Fig. S2B), respectively. The water contact angle of the substrate was significantly altered by the encapsulation of collagen (Fig. S2C), indicating a change in surface chemical properties.

We assessed the potential of IMRC expansion on HA-NHS ester, HA-COL, HAMC, and commercial microcarriers under static culture conditions (Table 1, Fig. S3). HAMC100 (HA microspheres coating 100 μg/mL

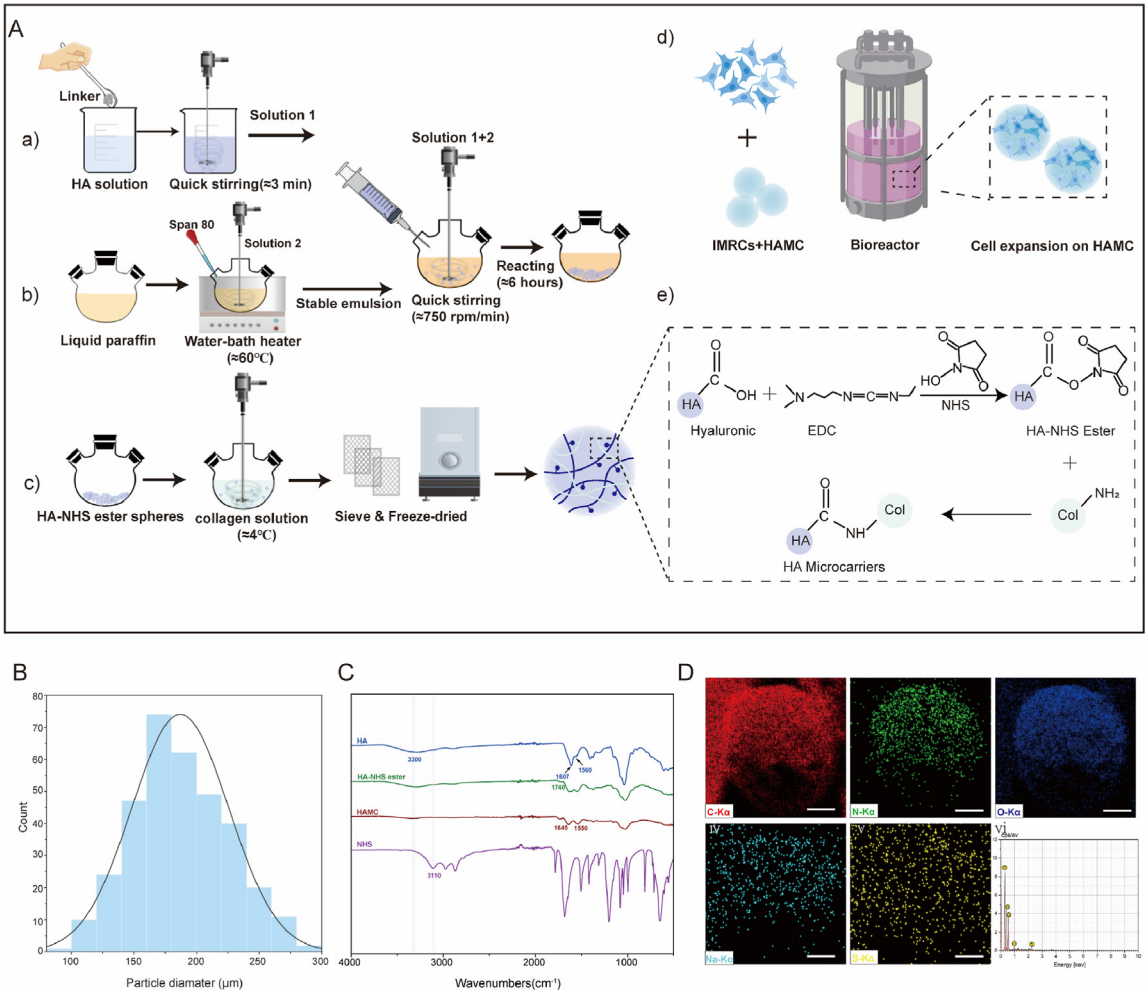

Fig. 1. Synthesis and characterisation of HA microcarriers (HAMCs). A. Schematic diagram of the preparation of HAMCs and IMRC culture at large-scale (Created with BioRender.com). **a-c**) The preparation of hyaluronic acid microspheres using the oil-in-water emulsification method, with the preconfigured pre-crosslinked aqueous phase, to produce HA-NHS ester. The HA-NHS ester was encapsulated by type I collagen to prepare HAMC. **d**) IMRCs expansion on HAMC in the bioreactor. **e**) Schematic diagram of HAMC cross-linking. The formation of HA-NHS ester was achieved by EDC/NHS, followed by the condensation of carboxyl and amino groups of collagen type I to create amide bonds. **B**. Diagram of HAMC particle size. **C**. FTIR Spectroscopy analysis of HA, HA-NHS ester, HAMC, and NHS. **D**. Elemental mapping of HAMC.

Table 1
Properties of commercially available microcarriers.

Microcarrier	Manufacturer	Material	Surface feature	Density (g/cm^3)	Bead size (μm)	Surface area (cm^2/g)	Carrier porosity
SoloHill	Sigma	Polystyrene	Collagen	1.02–1.03	125-212 and 150–210	325	Non-porous
m-Dev45	Corning	Polystyrene	Collagen	1.022–1.030	125–212	360	Non-porous
Cytodex-3	GE Healthcare	Dextran	Collagen	1.04	120–180	2000	Non-porous
Cultispher	Thermo Scientific	Gelatin	Uncoated	1.02–1.04	130–380	–	Macroporous

collagen concentration), along with m-Dev45, Cytodex-3, SoloHill and Cultispher, supported the expansion of IMRCs (Fig. S4A). Cultispher, identified as porous microcarrier, while HAMC100 and others supported cell growth on their surface. Live/dead assays demonstrated that several microcarriers facilitated attachment and survival; however, larger m-Dev4 microcarrier-cell agglomerates on day 4 may have resulted in cell apoptosis and decreased cell viability (Fig. S4A, Table S1). Harvesting cells with Tryple digestion showed that different microcarriers led to varying cumulative population doublings in IMRCs, with HAMC100 displaying superior cell expansion multiples and viability (Fig. S4B, Table S1). Microcarrier-expanded IMRCs retained their surface markers (Fig. S4C) and met the criteria established by the International Society of Cell Therapy (ISCT) [38]. Therefore, HAMC100 with HA as the core material, available in different particle sizes, shows good biocompatibility and supports the attachment and survival of IMRCs under static culture conditions.

3.2. *Microcarrier optimisation for dynamic culture in scalable bioreactors*

In this study, we utilised the industry-compatible DASbox Mini Bioreactor System, previously demonstrated for the efficient differentiation and cultivation of macrophages [39], to transfer monolayer cell culture IMRCs (P4) for suspension culture (Fig. 2A). The system allowed for computer-controlled maintenance of optimal physical conditions for the cell culture process, including DO (40%) and pH (7.2). Over a 7-day suspension culture period, daily samples were taken to assess cell

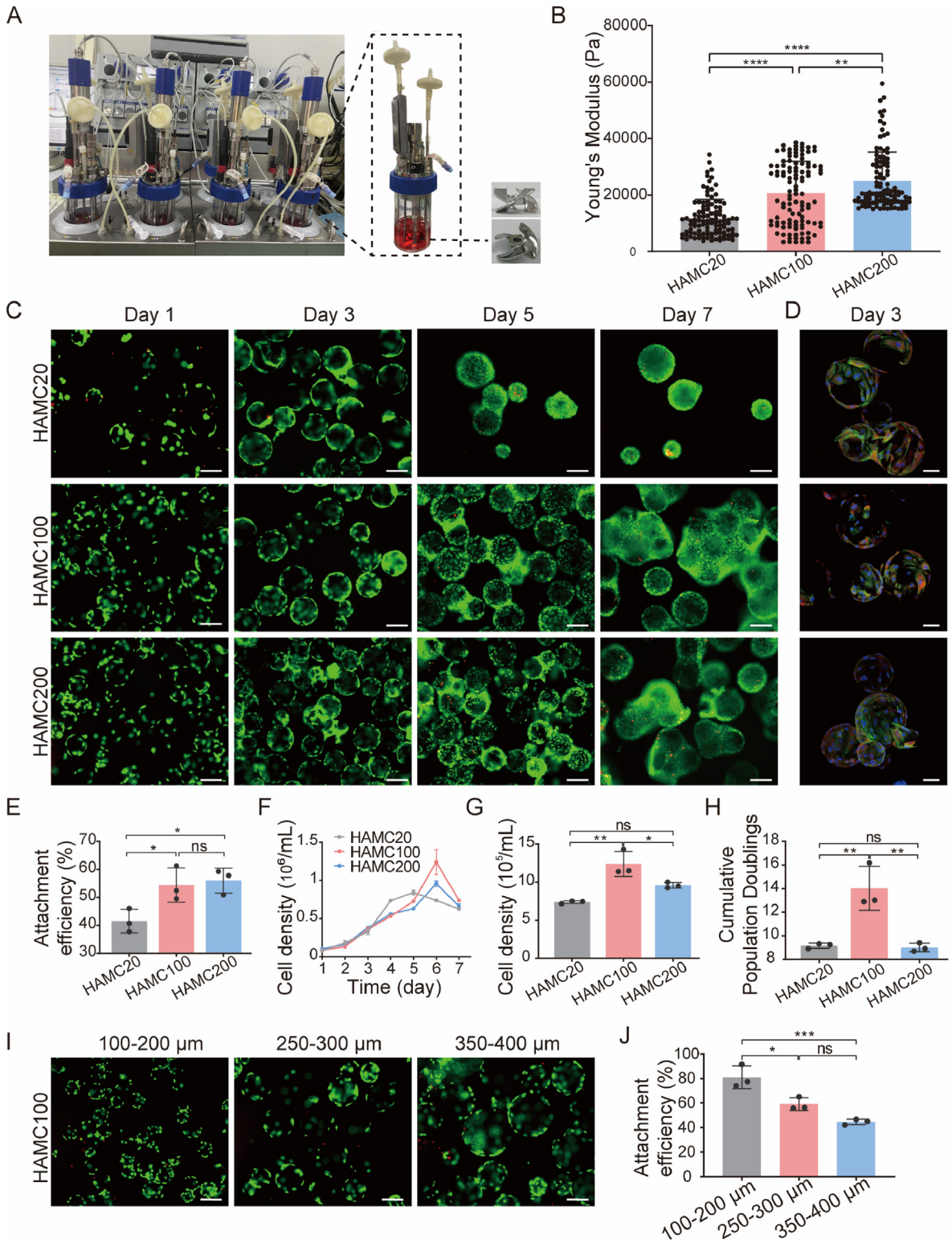

Fig. 2. IMRCs expanded on HAMC coated with different collagen concentrations or particle sizes in bioreactors. A. Photographs of the DASbox system and individual bioreactor filled with culture suspension (left). Pictures of the 3-blade impeller (right). **B**. Young's modulus of HAMC modified with different collagen concentrations (HAMC20, HAMC100 and HAMC200) analysed by AFM. **C**. Live/dead staining of IMRCs on HAMC20, HAMC100 and HAMC200 after 1 day, 3 days, 5 days and 7 days. Green indicates live cells, and red indicates dead cells. Scale bar, 200 μm. **D**. Cytoskeleton, focal adhesion and nucleus were imaged by rhodamine phalloidin (green), vinculin (red) and DAPI (blue). Scale bar, 50 μm. **E**. Attachment efficiency of IMRCs cultured for 24 h on HAMC20, HAMC100 and HAMC200. **F**. Growth curves of IMRCs cultured on HAMC20, HAMC100 and HAMC200 in bioreactors. **G**. Cell density of IMRCs cultured on HAMC20, HAMC100 and HAMC200 after 6 days in bioreactors. **H**. Cumulative population doublings of IMRCs cultured on HAMC20, HAMC100 and HAMC200 after 6 days. **I**. Live/dead staining of IMRCs on HAMC with different diameter ranges after 1 day. Green indicates live cells, and red indicates dead cells. Scale bar, 200 μm. **J**. Attachment efficiency of IMRCs cultured for 24 h on HAMC with different diameter ranges in bioreactors. (For interpretation of the references to color in this figure legend, the reader is referred to the Web version of this article.)

adhesion and expansion. In addition, to optimise HAMCs and their suitability for IMRC expansion in stirred bioreactors, we screened the microcarriers' cross-linking collagen concentration and particle size.

The surface modification of microcarriers is critical for cell adhesion, spreading and proliferation. Collagen has been shown to coat microcarriers to promote cell adhesion [40,41] effectively. To optimise HAMCs for the expansion of IMRCs in stirred bioreactors, we tested different collagen concentrations (20, 100, and 200 μg/mL) to coat the HA microspheres and evaluated the attachment efficiency of IMRCs after 24 h of inoculation in a stirred bioreactor. Using atomic force microscopy (AFM), we measured the local Young's moduli of HAMC20, HAMC100, and HAMC200 to be 11.78, 20.74, and 24.99 kPa, respectively (Fig. 2B). The cell attachment efficiency of IMRCs on HAMC100 and HAMC200 were significantly higher than that of HAMC20 (Fig. 2E and F). Cells continued to increase until the 6th day in the suspension culture process, with the highest cell densities of IMRCs on HAMC20, HAMC100, HAMC200 being 7.45×10^5 cells/mL, 1.24×10^6 cells/mL, and 9.59×10^5 cells/mL, respectively. HAMC100 achieved the highest cell density and population doubling of IMRCs, significantly higher than those on HAMC20 and HAMC200 (Fig. 2G, H, I).

Microcarrier size and curvature can affect cell adhesion and proliferation [23,42]. To determine the optimal particle size range of HAMC100 for IMRC attachment and expansion, we obtained microcarriers ranging from 100 to 200 μm, 250–300 μm, and 350–400 μm using screens with different pore sizes (Fig. 2I). After 24 h of inoculation in a stirred bioreactor, the cell attachment efficiencies of IMRCs were 81.02%, 55.87%, and 55.53% for the respective size ranges. Furthermore, higher cell attachment efficiency was observed on 100–200 μm HAMC100 compared to 250–300 μm and 350–400 μm (Fig. 2J). Therefore, 100–200 μm HAMC100 is a promising microcarrier for the large-scale culture of IMRCs in stirred bioreactors due to its superior adhesion and proliferation properties.

3.3. Cell characteristics and immunomodulatory potential of IMRCs on HAMCs in bioreactors

IMRCs derived from hESCs exhibit MSC-like characteristics and functions [9]. We evaluated cell properties and immunomodulatory potential of HAMC (100–200 μm HAMC100)-expanded IMRCs. On day 6 of culture, IMRCs were harvested from the bioreactors for the analyses of surface markers, karyotype stability, cell size, and cell viability. HAMC-expanded IMRCs showed >95% expression of positive MSC-specific surface markers (CD73, CD29, CD90, CD105 and HLA-ABC) and <1% expression of negative markers (CD45, CD34 and HLA-DR) (Fig. 3A). Karyotype analysis confirmed normal chromosome morphology and number, indicating genomic stability of microcarrier-expanded cells (Fig. 3B). IMRCs expanded on microcarriers and in monolayer culture, exhibited similar cell sizes and cryopreservation resistance (Fig. 3C and D). After freezing in liquid nitrogen, the thawed cells showed cell viability above 94% within 24 h at 4 °C (Fig. 3D). We utilised IMRC-laden microcarriers to verify their potential for trilineage differentiation in differentiating media. Our results showed that the IMRC-laden microcarriers were able to differentiate into adipogenic, osteogenic, and chondrogenic lineages after 21 days of differentiation, as depicted in Fig. 3E. Moreover, we observed that the microcarriers could support long-term adhesion and differentiation without shedding, but tissue block formation was observed over a longer period.

The immunomodulatory properties of HAMC-expanded IMRCs were also confirmed. The activation of 2,3-dioxygenase (IDO) is a key mechanism by which MSCs inhibit lymphocytes. Therefore, the response of IDO to the proinflammatory cytokine IFN-γ is central to immunosuppression in vitro [43]. We performed IFN-γ stimulation experiments and inhibition of PBMC proliferation verification. HAMC-expanded IMRCs displayed similar characteristic morphological changes to monolayer-expanded cells after IFN-γ stimulation (Fig. 3F). The expression of *IDO1* was upregulated in both microcarrier- and monolayer-expanded IMRCs after 24 h of IFN-γ stimulation (Fig. 3G).

Furthermore, the inhibitory effects of HAMC-expanded IMRCs on activated PBMC proliferation were investigated, revealing significant inhibition of activated PBMC proliferation at a ratio of 1:2, regardless of their sources (Fig. 3H). Increasing IMRC concentration enhanced the inhibitory effect on PBMC proliferation (Fig. 3H). When IMRCs were co-cultured with activated PBMCs at a ratio of 1:2 or 1:100, ten proinflammatory cytokines IL-5, IL-2Rα, TNF-α, TNF-β, IFN-γ, IL-13, IL-2, IL-9, IL-3, and Eotaxin were significantly downregulated, while anti-inflammatory cytokines IL-1RA and TRAIL and the immunomodulatory cytokines LIF, cytotrophic factor FGF basic, VEGF, SCGF-β, SCF, and HGF were downregulated with decreasing IMRCs concentration (Fig. S5, Table S2). In general, HAMC-expanded IMRCs maintained the basic characteristics of cells and exhibited immunomodulatory functions similar to those of monolayer cells.

3.4. Comparative analysis of IMRCs cultured under different conditions

To assess the impact of culture conditions on IMRCs, we compared the attachment, expansion and maintenance of cell characteristics on different microcarriers, including HAMCs, commercial microcarriers, and monolayer cultures. Live/dead staining showed that Cytodex-3 had more dead cells than HAMCs (Fig. 4A and B), and HAMCs had a higher attachment rate at 3 h post-inoculation in stirred bioreactors (Fig. 4C). In addition, a significantly lower attachment rate was observed on Cytodex-3 than on HAMCs at 3 h post-inoculation in stirred bioreactors (Fig. 4C). Dynamic culture of IMRCs with microcarriers showed that the highest cell density of HAMCs was significantly higher than that of Cytodex-3 (Fig. 4D and E). Harvested cells from microcarriers and monolayers were characterised by flow cytometry and trilineage differentiation ability. We found that IMRCs maintained a positive immunophenotype for the expression of CD29, CD73, CD105, HLA-ABC, and CD90 and negative for CD11b, CD19, and CD34 (Table 2) and the ability to differentiate into adipogenic, osteogenic, and chondrogenic lineages. However, cells expanded on Cytodex-3 exhibited lower Alizarin Red S staining than the other two groups, indicating lower osteogenic differentiation potential (Fig. 4F). Regarding cell proliferation and adhesion efficiency, HAMCs were more suitable for IMRCs than Cytodex-3 (Fig. 4G). The cells showed good morphology and no significant difference in cell adhesion efficiency and β-gal activity compared to monolayer cells (Fig. 4H and I). Moreover, HAMCs exhibited significantly higher proliferative ability than Cytodex-3 (Fig. 4G). These findings suggest that HAMCs provide a more favourable microenvironment for IMRC adhesion, proliferation, and osteogenic differentiation than Cytodex-3.

To further investigate the gene expression differences between IMRCs cultured on different microcarriers and in monolayer culture, we performed RNA-seq analysis. PCA results showed clustering of monolayer and microcarrier groups, indicating that the gene expression pattern may differ at the mRNA level (Fig. 5A). Differentially expressed gene (DEG) analysis revealed the upregulation of 634 genes and the downregulation of 222 genes in microcarrier groups compared to the monolayer group (Fig. 5B). A heatmap of DEGs between monolayer and microcarrier-amplified IMRCs showed that some genes were upregulated in the microcarrier groups compared to the monolayer group (Fig. 5C). Specifically, MSC markers such as *SPARC*, *NT5E* (*CD73*), and *ENG* (*CD90*) were upregulated in the microcarrier group, while *BMP2*, associated with osteoblastic and chondrogenic differentiation, was highly expressed in HAMC-amplified cells. The expression patterns of the cell extracellular matrix (ECM) were different between the microcarrier and monolayer groups. IMRCs in suspension culture on microcarriers generally secreted more ECM, especially collagen-related protein expression. HAMC-expanded cells highly expressed *osteoglycin* (*OGN*), *COL2A1* and *PRG4*, which are more conducive to bone formation and cartilage development.

Furthermore, we conducted a Gene Ontology (GO) enrichment analysis to identify the correlation between the DEGs and important

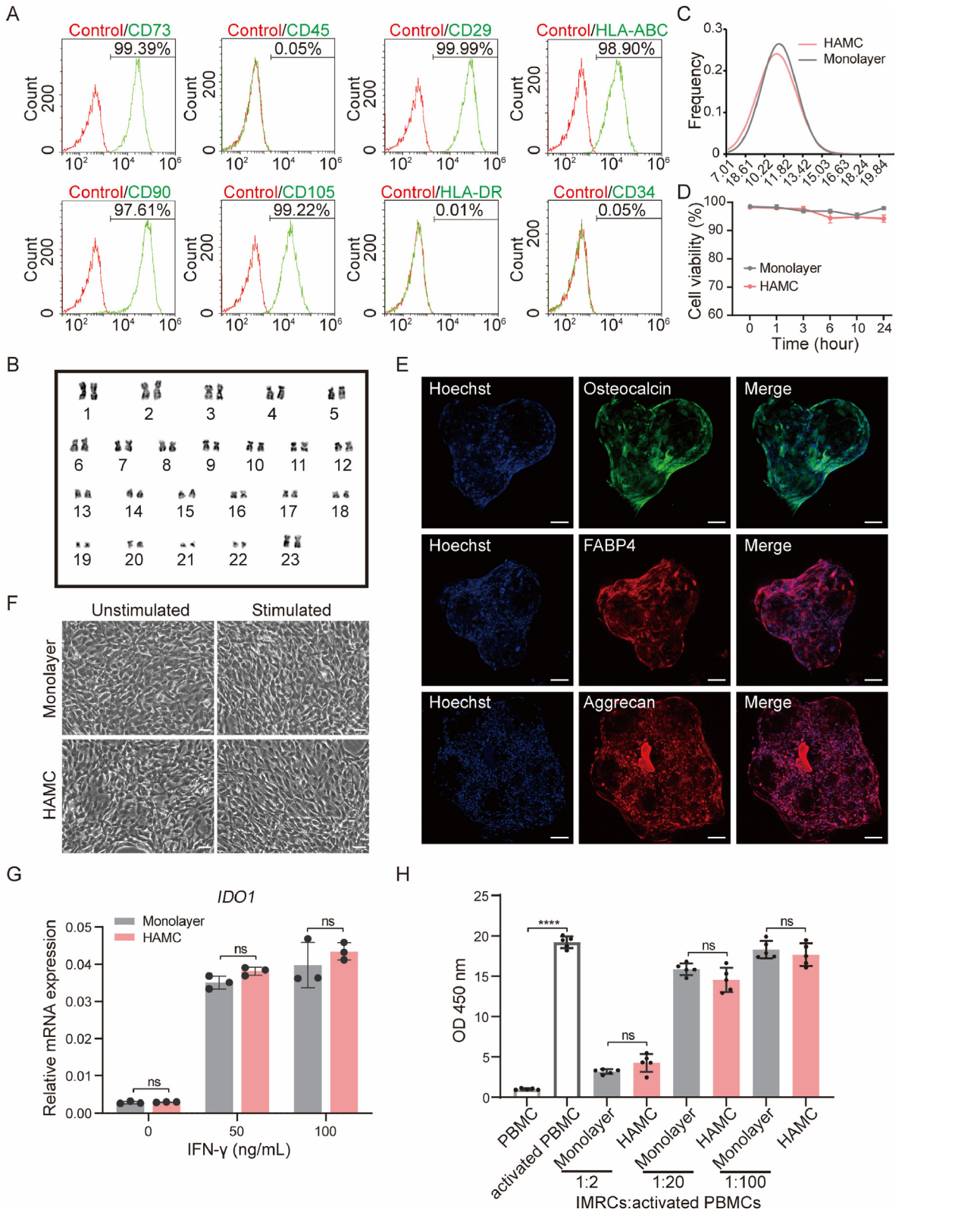

Fig. 3. IMRCs expanded on HAMCs maintain cell stemness and immunomodulatory capabilities in stirred bioreactors. A. MSC-specific markers of IMRCs harvested from HAMCs (100–200 μm HAMC100). Isotype antibodies were used as controls for gating. **B**. Karyotyping of IMRCs harvested from HAMC. **C**. Distribution of cell diameters of IMRCs harvested from monolayer culture or HAMCs expansion. **D**. Viability of IMRCs harvested from monolayers or HAMC in clinical injection buffer over time at 4 °C. **E**. Representative immunofluorescence staining of IMRC-laden microcarriers in situ after they were induced to undergo osteogenic differentiation (osteocalcin), adipogenic differentiation (FABP-4), and chondrogenic differentiation (aggrecan). Scale bar, 100 μm. **F**. Morphology of IMRCs harvested from monolayers and HAMCs before and after IFN-γ stimulation. Scale bar, 100 μm. **G**. Real-time qPCR for *IDO1* mRNA in IMRCs harvested from monolayers and HAMCs before and after IFN-γ (0, 50 and 100 ng/mL) treatment. **H**. The inhibitory effects of IMRCs on activated PBMC (CD3/28 and IL-2 costimulated) proliferation at ratios of 1:2, 1:20 and 1:100 in vitro.

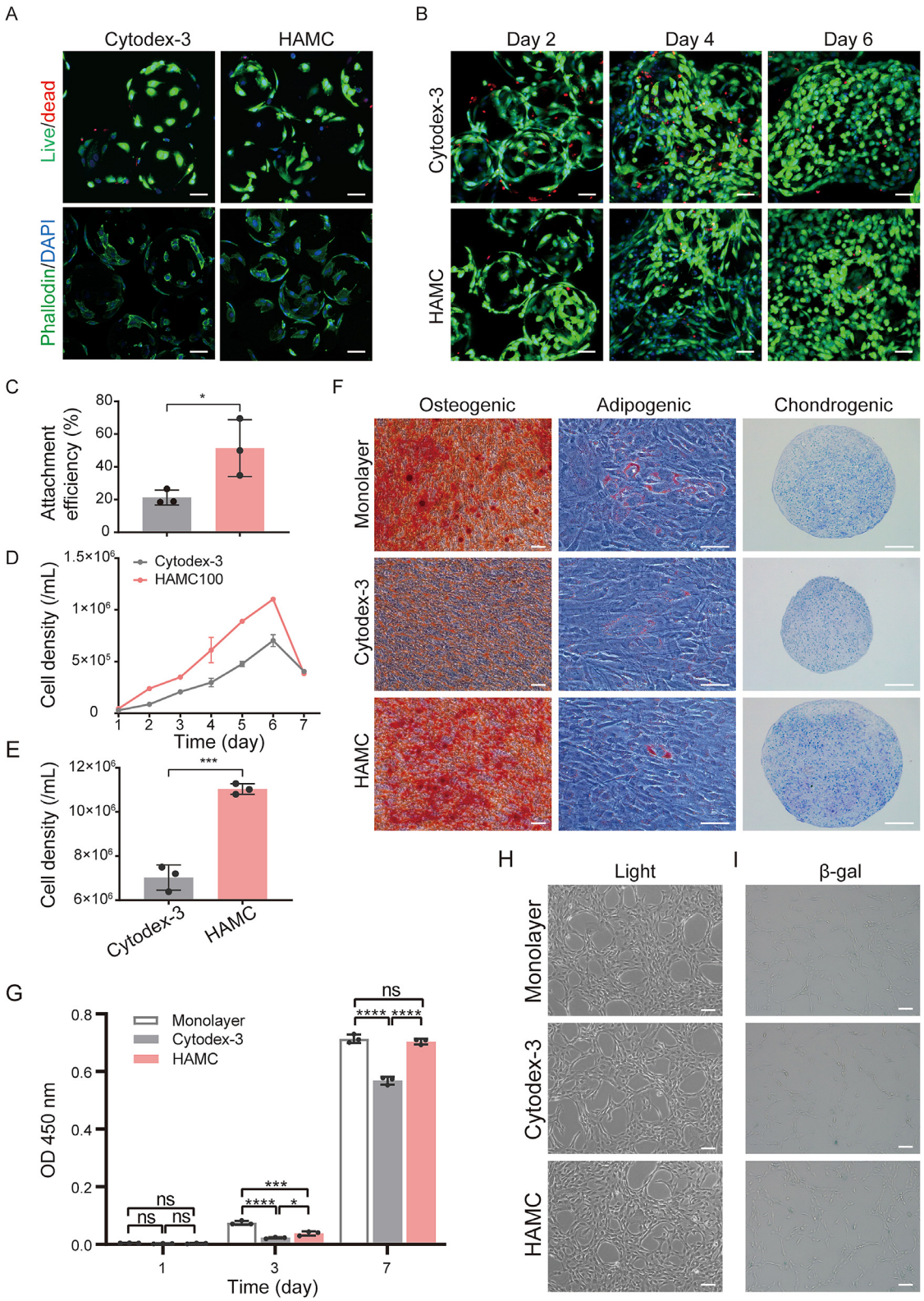

Fig. 4. Differences in cell characteristics of IMRCs cultured on monolayers and different microcarriers in stirred bioreactors. A. Live/dead and phalloidin/DAPI staining of IMRCs on different microcarriers at 3 h (Green: live cells, cytoskeleton; red: dead cells; blue: cell nucleus). Scale bar, 50 μm. **B**. Live/dead staining of IMRCs on different microcarriers after 2 days, 4 days, and 6 days. (Green: live cells, red: dead cells). Scale bar, 50 μm. **C**. Attachment efficiency of IMRCs cultured for 3 h in bioreactors. **D**. Growth curves of IMRCs cultured on different microcarriers in bioreactors. **E**. Cell density of IMRCs cultured on different microcarriers after 6 days in bioreactors. **F**. Multipotency of IMRCs harvested from monolayers or microcarriers was examined by differentiation into osteogenic, adipogenic and chondrogenic lineages. Scale bar, 100 μm. **G**. Cell proliferation of IMRCs harvested from monolayers or microcarriers and cultured in cell culture plates. **H**. Cell adhesion and morphology of IMRCs harvested from monolayers or microcarriers and inoculated into cell culture plates. Scale bar, 100 μm. **I**. Cell senescence detection by β-galactosidase (β-gal) staining of monolayers or different microcarriers. Scale bar, 100 μm. (For interpretation of the references to color in this figure legend, the reader is referred to the Web version of this article.)

Table 2
Flow cytometry analysis of surface markers of IMRCs expanded on monolayers and microcarriers.

Markers (%)	CD11b -	CD19 -	CD29 +	CD34 -	CD73 +	CD105 +	HLA-ABC +	CD90 +
Monolayer-IMRCs	0.11	0.42	100.00	0.01	99.85	99.99	100.00	99.85
Cytodex-3-IMRCs	0.08	0.01	99.97	0.16	99.08	99.78	99.98	98.05
HAMCs-IMRCs	0.11	0.03	100.00	0.04	99.30	99.90	99.97	97.65

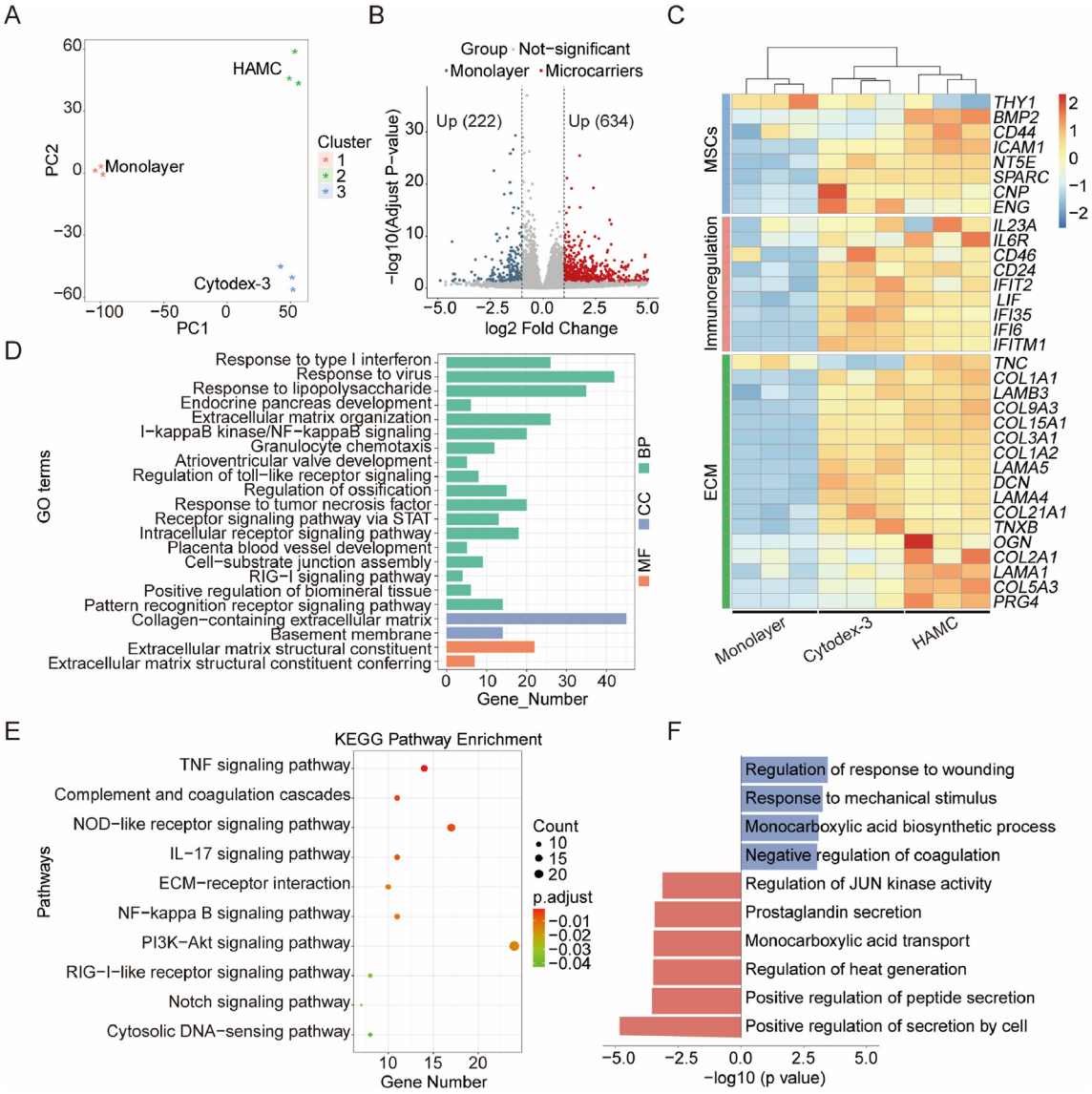

Fig. 5. Transcriptome profiles of IMRCs harvested from monolayers or microcarriers in stirred bioreactors. A. Principal component analysis (PCA) of RNA-Seq of the monolayer group and microcarrier groups. **B.** Volcano map of differentially expressed genes (DEGs) of IMRCs harvested from microcarriers vs. monolayer. Blue dots indicate significantly downregulated DEGs; red dots indicate significantly upregulated DEGs; grey dots indicate no significant difference. **C.** Heatmap of DEGs in IMRCs among the monolayer group and different microcarrier groups. **D.** GO terms of microcarrier groups. BP, biological processes; CC, cellular component; MF, molecular function. **E.** KEGG pathway enrichment of microcarrier groups. The black number is the number of enriched genes. **F.** GO terms of the Cytodex-3 group vs. HAMC group. (For interpretation of the references to color in this figure legend, the reader is referred to the Web version of this article.)

biological processes and pathways (Fig. 5D). The GO analysis revealed that DEGs in the microcarrier groups were mainly associated with biological processes such as response to type I interferon, response to virus, response to lipopolysaccharide, and extracellular matrix organization. In addition, KEGG analysis showed that the upregulated DEGs between the microcarrier and monolayer groups were enriched in 10 pathways, including the TNF signalling pathway, ECM-receptor interaction, and PI3K-Akt signalling pathway (Fig. 5E). Moreover, the GO analysis revealed that DEGs in the Cytodex-3 group were mainly related to the regulation of response to wounding, response to mechanical stimulus, monocarboxylic acid biosynthetic process, and negative regulation of coagulation. In contrast, DEGs in the HAMC group were mainly related to the regulation of JUN kinase activity, prostaglandin secretion, monocarboxylic acid transport, regulation of heat generation, positive regulation of peptide secretion, and positive regulation of secretion by cell (Fig. 5F). Furthermore, it was observed that the HAMC-amplified cells

exhibited a stronger secretion ability compared to the Cytodex-3 group.

3.5. HAMC surface structure optimisation for IMRCs dynamic culture in bioreactors

To improve the cell loading capacity of individual microcarriers and scale up cell production, we optimised HAMCs to obtain microcarriers with concave structures (cHAMCs). This was achieved by adding ammonium bicarbonate, which produced many bubbles that adhered to the surface of the uncrosslinked microcarriers to form a unique concave structure. The cHAMCs had a concave-shaped surface in both dry and wet conditions, with an average depression width of approximately 30 μm which allowed for cell growth (Fig. 6A). The concave structure on the surface of the microcarriers remained stable, and the length of depressions of cHAMCs was between 20 and 30 μm (Fig. 6B).

In suspension culture, cells maintained good survival on both HAMCs and cHAMCs (Fig. 6C). However, the cell attachment efficiency of IMRCs on cHAMCs was significantly higher than those on HAMCs (Fig. 6D). The kinetic growth curves showed that cHAMCs consistently had a higher cell volume than HAMCs, with a culture density of 1.48×10^6 cells/mL on the 6th day (Fig. 6E and F). Nevertheless, the cells could maintain good cell viability on both kinds of microcarriers with different morphologies (Fig. 6G). We also evaluated the concentrations of nutrient glucose and lactic acid production as metabolic waste in the culture process. The results showed that the cHAMCs had higher glucose consumption and lactic acid production, consistent with the cell density (Fig. 6H and I). These findings suggest that cHAMCs could improve cell adhesion ability and yield compared to HAMCs.

4. Discussion

In this study, we investigated hyaluronic acid-based microcarriers (HAMCs) for the scalable suspension culture of IMRCs in a stirred bioreactor. Our results demonstrated that HAMCs could support IMRC expansion in serum-free conditions without compromising cell proliferation, differentiation potential or immune regulation. In addition, microcarrier optimisation was performed, and HAMC100 with a size range of 100–200 μm exhibited the best cell attachment and expansion capabilities.

The seeding efficiency of MSCs ranged from 10% to 60% after 18 h of

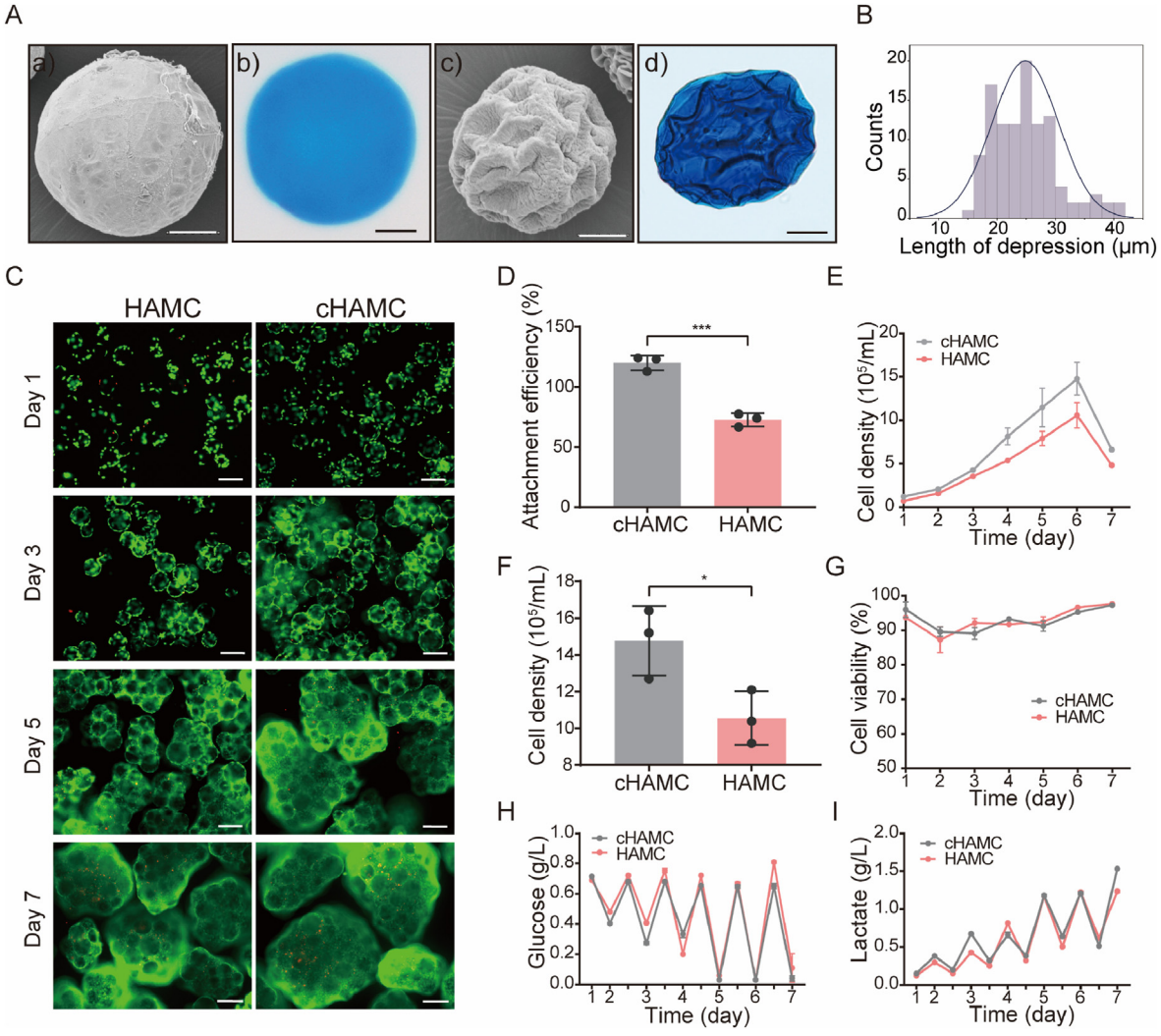

Fig. 6. IMRCs expanded on HAMCs and concave-structured HAMCs (cHAMCs) in bioreactors. A. The characteristics of HAMCs and cHAMCs. **a**, **c**) SEM images of HAMCs and cHAMCs. HAMCs have a smooth surface, while cHAMCs have a concave structure. Scale bar, 200 μm. **b**, **d**) Morphological characteristics of HAMCs and cHAMCs in wet conditions. **B**. Distribution of depression length in cHAMCs. **C**. Live/dead staining of IMRCs on HAMCs and cHAMCs after 1 day, 3 days, 5 days, and 7 days. Green indicates live cells, and red indicates dead cells. Scale bar, 200 μm. **D**. Attachment efficiency of IMRCs cultured for 24 h on HAMCs and cHAMCs in bioreactors. **E**. Growth curves of IMRCs cultured on HAMCs and cHAMCs in bioreactors. **F**. Cell density of IMRCs cultured on HAMCs and cHAMCs after 6 days in bioreactors. **G**. Viability of IMRCs cultured on HAMCs and cHAMCs in bioreactors. **H**. Glucose concentration of cells in the culture supernatant. **I**. Lactate production of cells in the culture supernatant. (For interpretation of the references to color in this figure legend, the reader is referred to the Web version of this article.)

seeding with different microcarriers in a previous study [44]. In our study, the cell attachment efficiencies of IMRCs on the prepared HAMCs were 56.02% and 81.02% at 3 and 24 h post-inoculation under dynamic culture conditions, respectively. These results were superior to those obtained on collagen-coated Cytodex-3, a commercial microcarrier.

Different types of microcarriers have been categorised into nonporous, microporous and macroporous types [25]. While macroporous microcarriers can provide a larger surface area for cell attachment and growth, they may also result in hypoxia or apoptosis due to limited oxygen and nutrient supply in the core, negatively affecting cell viability [2]. In our study, we developed a new type of microcarrier, cHAMC, with a concave surface that could provide a larger surface area to support cell growth on the microcarrier surface. The concave structure of cHAMCs may provide more adhesion sites to improve the cell adhesion rate of the microcarrier and even cause the cells to enter cell expansion earlier, which is a potential microcarrier model. In addition to being used for large-scale culture, cell-laden cHAMCs could also be directly transplanted in situ for treatment, and microcarriers could play the role of cell fixation.

RNA-seq analysis of IMRCs amplified by different microcarriers or in a monolayer revealed different gene expression patterns. This may be because different core materials, different substrate surfaces, and different sizes may affect the stiffness, curvature, etc., of the microcarriers, resulting in different cellular responses [2,45]. IMRCs expanded on HAMCs and Cytodex-3 showed higher expression of ECM-related genes than cells grown in monolayer culture. In addition, compared with Cytodex-3 IMRCs, IMRCs expanded on HAMCs had higher cell secretion ability and high expression of *BMP2*, *OGN*, *COL2A1*, and *PRG-4*, which may be more conducive to osteogenic differentiation, chondrogenic differentiation, and endochondral ossification in stem cells [46–49]. Therefore, different microcarriers should be customised according to various research purposes or requirements to obtain cell populations with tendencies that achieve better results in future studies.

Since the target of cell therapy products is the cells themselves, efficient cell harvesting after cell expansion is critical [50]. Detachment of cells from the surface of non-degradable microcarriers is usually performed by enzymatic digestion, and the cells are separated from the microcarriers through sterile sieves or filtration device [51]. During this process, may suffer not only protease contamination and poor yield of cell detachment, but also microcarrier debris smaller than the filter aperture may be generated, potentially contaminating cell therapy products [51,52]. HAMC and cHAMC, as non-degradable microcarriers, traditional enzymatic digestion is still required in the cell harvesting process, which may face these problems in larger volumes of large-scale expansion. In previous studies, dissolvable microcarriers have been applied to manufacture MSCs, releasing cells by completely degrading microcarriers, simplifying the downstream purification process, and reducing cell loss in the cell harvesting step [53,54]. Therefore, the cell detachment method and degradability of HAMCs still need to be further studied to solve the limitations of HAMCs and cHAMCs in follow-up studies. Furthermore, further optimisation is needed in the preparation of HAMCs and cHAMCs using the emulsification method to enhance the production of microcarriers for large-scale applications.

Conclusively, our research demonstrates that HAMCs and cHAMCs have the potential to be a valuable tool for the large-scale production of stem cells in bioreactor-based systems. This could greatly enhance the efficiency and scalability of stem cells, making them a promising option for various biomedical applications.

Author contributions

Conceptualisation, QG, TTG, XYZ, and JH; Methodology, TTG, XYZ; Resources, JH, WJL; Data Acquisition, TTG, XYZ, HKM, BA, FGS, SSL, BJG, SSN, CXW; Data Analysis and Interpretation, TTG, XYZ, YT, ZWL, GHF; Visualization, TTG, XYZ, YT; Writing-Original Draft Preparation, TTG; Writing-Review & Editing, TTG, XYZ, QG, JW; Project administration and Supervision, QG, QZ, MJG, JW, JH, YKW, LW, WL.

Declaration of competing interest

The authors declare that they have no known competing financial interests or personal relationships that could have appeared to influence the work reported in this paper.

Data availability

Data will be made available on request.

Acknowledgements

We appreciate Qi Zhou for his dedicated support to this project. Chunli Li from Instrument Center of Institute of Microbiology, Chinese Academy of Sciences with SEM measurements is also appreciated. This work was supported by the National Key Research and Development Program (2019YFA0110900, 2021YFA1101600, 2020YFA0804000, 2018YFE0204400, 2018YFA0108500, 2018YFC2000100, 2019YFA0110100), Strategic Priority Research Program of Chinese Academy of Sciences (XDA16020802, XDA16021102, XDA16030701/702, XDA16040502/504), Beijing Institute for Stem Cell and Regenerative Medicine Project Incubation Found (2022FH110, 2022FH117), National Natural Science Foundation of China (T2222029 and U21A20396), the international cooperation project of China Manned Space Program, CAS Project for Young Scientists in Basic Research (YSBR-012), CAS Engineering Laboratory for Intelligent Organ Manufacturing (KFJ-PTXM-039).

Appendix A. Supplementary data

Supplementary data to this article can be found online at https://doi.org/10.1016/j.mtbio.2023.100662.

References

[1] J. Wang, L. Liao, J. Tan, Mesenchymal-stem-cell-based experimental and clinical trials: current status and open questions, Expet Opin. Biol. Ther. 11 (7) (2011) 893–909, https://doi.org/10.1517/14712598.2011.574119.
[2] H. Tavassoli, S.N. Alhosseini, A. Tay, P.P.Y. Chan, S.K. Weng Oh, M.E. Warkiani, Large-scale production of stem cells utilising microcarriers: a biomaterials engineering perspective from academic research to commercialised products, Biomaterials 181 (2018) 333–346, https://doi.org/10.1016/j.biomaterials.2018.07.016.
[3] A. Brooks, K. Futrega, X. Liang, X. Hu, X. Liu, D.H.G. Crawford, M.R. Doran, M.S. Roberts, H. Wang, Concise review: quantitative detection and modeling the in vivo kinetics of therapeutic mesenchymal stem/stromal cells, Stem Cells Transl Med 7 (1) (2018) 78–86, https://doi.org/10.1002/sctm.17-0209.
[4] H. Inoue, N. Nagata, H. Kurokawa, S. Yamanaka, iPS cells: a game changer for future medicine, EMBO J. 33 (5) (2014) 409–417, https://doi.org/10.1002/embj.201387098.
[5] Y. Wang, L. Cheng, S. Gerecht, Efficient and scalable expansion of human pluripotent stem cells under clinically compliant settings: a view in 2013, Ann. Biomed. Eng. 42 (7) (2014) 1357–1372, https://doi.org/10.1007/s10439-013-0921-4.
[6] C. Kropp, D. Massai, R. Zweigerdt, Progress and challenges in large-scale expansion of human pluripotent stem cells, Process Biochem. 59 (2017) 244–254, https://doi.org/10.1016/j.procbio.2016.09.032.
[7] T.-M. Liu, Application of mesenchymal stem cells derived from human pluripotent stem cells in regenerative medicine, World J. Stem Cell. 13 (12) (2021) 1826–1844, https://doi.org/10.4252/wjsc.v13.i12.1826.
[8] B. Jiang, L. Yan, X. Wang, E. Li, K. Murphy, K. Vaccaro, Y. Li, R.-H. Xu, Concise review: mesenchymal stem cells derived from human pluripotent cells, an unlimited and quality-controllable source for therapeutic applications, Stem Cell. 37 (5) (2019) 572–581, https://doi.org/10.1002/stem.2964.
[9] J. Wu, D. Song, Z. Li, B. Guo, Y. Xiao, W. Liu, L. Liang, C. Feng, T. Gao, Y. Chen, Y. Li, Z. Wang, J. Wen, S. Yang, P. Liu, L. Wang, Y. Wang, L. Peng, G.N. Stacey, Z. Hu, G. Feng, W. Li, Y. Huo, R. Jin, N. Shyh-Chang, Q. Zhou, L. Wang, B. Hu, H. Dai, J. Hao, Immunity-and-matrix-regulatory cells derived from human embryonic stem cells safely and effectively treat mouse lung injury and fibrosis, Cell Res. 30 (9) (2020) 794–809, https://doi.org/10.1038/s41422-020-0354-1.
[10] D. Xing, K. Wang, J. Wu, Y. Zhao, W. Liu, J.J. Li, T. Gao, D. Yan, L. Wang, J. Hao, J. Lin, Clinical-grade human embryonic stem cell-derived mesenchymal stromal

cells ameliorate the progression of osteoarthritis in a rat model, Molecules 26 (3) (2021), https://doi.org/10.3390/molecules26030604.
[11] J. Liu, Z. Hou, J. Wu, K. Liu, D. Li, T. Gao, W. Liu, B. An, Y. Sun, F. Mo, L. Wang, Y. Wang, J. Hao, B. Hu, Infusion of hESC derived Immunity-and-matrix regulatory cells improves cognitive ability in early-stage AD mice, Cell Prolif. 54 (8) (2021), e13085, https://doi.org/10.1111/cpr.13085.
[12] J. Wu, X. Zhou, Y. Tan, L. Wang, T. Li, Z. Li, T. Gao, J. Fan, B. Guo, W. Li, J. Hao, X. Wang, B. Hu, Phase 1 trial for treatment of COVID-19 patients with pulmonary fibrosis using hESC-IMRCs, Cell Prolif. 53 (12) (2020), e12944, https://doi.org/10.1111/cpr.12944.
[13] J. Wu, Z. Hu, L. Wang, Y. Tan, W. Hou, Z. Li, T. Gao, J. Fan, B. Guo, H. Dai, W. Li, J. Hao, R. Jin, B. Hu, First case of COVID-19 infused with hESC derived immunity-and matrix-regulatory cells, Cell Prolif. 53 (12) (2020), e12943, https://doi.org/10.1111/cpr.12943.
[14] C.A.V. Rodrigues, T.G. Fernandes, M.M. Diogo, C.L. da Silva, J.M.S. Cabral, Stem cell cultivation in bioreactors, Biotechnol. Adv. 29 (6) (2011) 815–829, https://doi.org/10.1016/j.biotechadv.2011.06.009.
[15] M.J. Jenkins, S.S. Farid, Human pluripotent stem cell-derived products: advances towards robust, scalable and cost-effective manufacturing strategies, Biotechnol. J. 10 (1) (2015) 83–95, https://doi.org/10.1002/biot.201400348.
[16] J.M. Crook, T.T. Peura, L. Kravets, A.G. Bosman, J.J. Buzzard, R. Horne, H. Hentze, N.R. Dunn, R. Zweigerdt, F. Chua, A. Upshall, A. Colman, The generation of six clinical-grade human embryonic stem cell lines, Cell Stem Cell 1 (5) (2007) 490–494.
[17] V. Bunpetch, H. Wu, S. Zhang, H. Ouyang, From "bench to bedside": current advancement on large-scale production of mesenchymal stem cells, Stem Cell. Dev. 26 (22) (2017) 1662–1673, https://doi.org/10.1089/scd.2017.0104.
[18] A. Lavrentieva, A. Hoffmann, C. Lee-Thedieck, Limited potential or unfavorable manipulations? Strategies toward efficient mesenchymal stem/stromal cell applications, Front. Cell Dev. Biol. 8 (2020) 316, https://doi.org/10.3389/fcell.2020.00316.
[19] D.A. Castilla-Casadiego, A.M. Reyes-Ramos, M. Domenech, J. Almodovar, Effects of physical, chemical, and biological stimulus on h-MSC expansion and their functional characteristics, Ann. Biomed. Eng. 48 (2) (2020) 519–535, https://doi.org/10.1007/s10439-019-02400-3.
[20] P. Silva Couto, M.C. Rotondi, A. Bersenev, C.J. Hewitt, A.W. Nienow, F. Verter, Q.A. Rafiq, Expansion of human mesenchymal stem/stromal cells (hMSCs) in bioreactors using microcarriers: lessons learnt and what the future holds, Biotechnol. Adv. 45 (2020), 107636, https://doi.org/10.1016/j.biotechadv.2020.107636.
[21] P. Jayaraman, R. Lim, J. Ng, M.C. Vemuri, Acceleration of translational mesenchymal stromal cell therapy through consistent quality GMP manufacturing, Front. Cell Dev. Biol. 9 (2021), 648472, https://doi.org/10.3389/fcell.2021.648472.
[22] M. Krukowski, D.J. Simmons, A. Summerfield, P. Osdoby, Charged beads: generation of bone and giant cells, J. Bone Miner. Res. 3 (2) (1988) 165–171.
[23] S. Derakhti, S.H. Safiabadi-Tali, G. Amoabediny, M. Sheikhpour, Attachment and detachment strategies in microcarrier-based cell culture technology: a comprehensive review, Mater Sci Eng C Mater Biol Appl 103 (2019), 109782, https://doi.org/10.1016/j.msec.2019.109782.
[24] Q.A. Rafiq, K. Coopman, A.W. Nienow, C.J. Hewitt, Systematic microcarrier screening and agitated culture conditions improves human mesenchymal stem cell yield in bioreactors, Biotechnol. J. 11 (4) (2016) 473–486, https://doi.org/10.1002/biot.201400862.
[25] B. Koh, N. Sulaiman, M.B. Fauzi, J.X. Law, M.H. Ng, R.B.H. Idrus, M.D. Yazid, Three dimensional microcarrier system in mesenchymal stem cell culture: a systematic review, Cell Biosci. 10 (2020) 75, https://doi.org/10.1186/s13578-020-00438-8.
[26] A. Fallacara, E. Baldini, S. Manfredini, S. Vertuani, Hyaluronic acid in the third millennium, Polymers (Basel) 10 (7) (2018), https://doi.org/10.3390/polym10070701.
[27] A. Fallacara, F. Marchetti, M. Pozzoli, U.R. Citernesi, S. Manfredini, Silvia Vertuani, Formulation and characterization of native and crosslinked hyaluronic acid microspheres for dermal delivery of sodium ascorbyl phosphate: a comparative study, Pharmaceutics 10 (4) (2018), https://doi.org/10.3390/pharmaceutics10040254.
[28] J.A. Burdick, G.D. Prestwich, Hyaluronic acid hydrogels for biomedical applications, Adv. Mater. 23 (12) (2011) H41–H56, https://doi.org/10.1002/adma.201003963.
[29] C.B. Highley, G.D. Prestwich, J.A. Burdick, Recent advances in hyaluronic acid hydrogels for biomedical applications, Curr. Opin. Biotechnol. 40 (2016) 35–40, https://doi.org/10.1016/j.copbio.2016.02.008.
[30] L. Yang, Y. Liu, X. Shou, D. Ni, T. Kong, Y. Zhao, Bio-inspired lubricant drug delivery particles for the treatment of osteoarthritis, Nanoscale 12 (32) (2020) 17093–17102, https://doi.org/10.1039/d0nr04013d.
[31] F. Mohand-Kaci, N. Assoul, I. Martelly, E. Allaire, M. Zidi, Optimised hyaluronic acid-hydrogel design and culture conditions for preservation of mesenchymal stem cell properties, Tissue Eng. C Methods 19 (4) (2013) 288–298, https://doi.org/10.1089/ten.TEC.2012.0144.
[32] Y.-J. Seong, G. Lin, B.J. Kim, H.-E. Kim, S. Kim, S.-H. Jeong, Hyaluronic acid-based hybrid hydrogel microspheres with enhanced structural stability and high injectability, ACS Omega 4 (9) (2019) 13834–13844, https://doi.org/10.1021/acsomega.9b01475.
[33] M. Hamilton, S. Harrington, P. Dhar, L. Stehno-Bittel, Hyaluronic acid hydrogel microspheres for slow release stem cell delivery, ACS Biomater. Sci. Eng. 7 (8) (2021) 3754–3763, https://doi.org/10.1021/acsbiomaterials.1c00658.
[34] S. Jiang, C. Lyu, P. Zhao, W. Li, W. Kong, C. Huang, G.M. Genin, Y. Du, Cryoprotectant enables structural control of porous scaffolds for exploration of cellular mechano-responsiveness in 3D, Nat. Commun. 10 (1) (2019) 3491, https://doi.org/10.1038/s41467-019-11397-1.
[35] C. Trapnell, B.A. Williams, G. Pertea, A. Mortazavi, G. Kwan, M.J. van Baren, S.L. Salzberg, B.J. Wold, L. Pachter, Transcript assembly and quantification by RNA-Seq reveals unannotated transcripts and isoform switching during cell differentiation, Nat. Biotechnol. 28 (5) (2010) 511–515, https://doi.org/10.1038/nbt.1621.
[36] S. Bagheri, Z. Bagher, S. Hassanzadeh, S. Simorgh, S.K. Kamrava, V.T. Nooshabadi, R. Shabani, M. Jalessi, M. Khanmohammadi, Control of cellular adhesiveness in hyaluronic acid-based hydrogel through varying degrees of phenol moiety cross-linking, J. Biomed. Mater. Res. 109 (5) (2021) 649–658, https://doi.org/10.1002/jbm.a.37049.
[37] C. Wang, Q. Yan, H.B. Liu, X.H. Zhou, S.J. Xiao, Different EDC/NHS activation mechanisms between PAA and PMAA brushes and the following amidation reactions, Langmuir 27 (19) (2011) 12058–12068, https://doi.org/10.1021/la202267p.
[38] M. Dominici, K. Le Blanc, I. Mueller, I. Slaper-Cortenbach, F. Marini, D. Krause, R. Deans, A. Keating, D. Prockop, E. Horwitz, Minimal criteria for defining multipotent mesenchymal stromal cells, Int. Soc. Cell. Ther. Position Statement, Cytotherapy 8 (4) (2006) 315–317.
[39] M. Ackermann, H. Kempf, M. Hetzel, C. Hesse, A.R. Hashtchin, K. Brinkert, J.W. Schott, K. Haake, M.P. Kühnel, S. Glage, C. Figueiredo, D. Jonigk, K. Sewald, A. Schambach, S. Wronski, T. Moritz, U. Martin, R. Zweigerdt, A. Munder, N. Lachmann, Bioreactor-based mass production of human iPSC-derived macrophages enables immunotherapies against bacterial airway infections, Nat. Commun. 9 (1) (2018) 5088, https://doi.org/10.1038/s41467-018-07570-7.
[40] C. Loubière, C. Sion, N. De Isla, L. Reppel, E. Guedon, I. Chevalot, E. Olmos, Impact of the type of microcarrier and agitation modes on the expansion performances of mesenchymal stem cells derived from umbilical cord, Biotechnol. Prog. 35 (6) (2019) e2887, https://doi.org/10.1002/btpr.2887.
[41] J.D. Krutty, A.D. Dias, J. Yun, W.L. Murphy, P. Gopalan, Synthetic, chemically defined polymer-coated microcarriers for the expansion of human mesenchymal stem cells, Macromol. Biosci. 19 (2) (2019), e1800299, https://doi.org/10.1002/mabi.201800299.
[42] C. Chung, J.A. Burdick, Influence of three-dimensional hyaluronic acid microenvironments on mesenchymal stem cell chondrogenesis, Tissue Eng Part A 15 (2) (2009) 243–254, https://doi.org/10.1089/ten.tea.2008.0067.
[43] M. Krampera, J. Galipeau, Y. Shi, K. Tarte, L. Sensebe, Immunological characterisation of multipotent mesenchymal stromal cells–The International Society for Cellular Therapy (ISCT) working proposal, Cytotherapy 15 (9) (2013) 1054–1061, https://doi.org/10.1016/j.jcyt.2013.02.010.
[44] D. Schop, R. van Dijkhuizen-Radersma, E. Borgart, F.W. Janssen, H. Rozemuller, H.J. Prins, J.D. de Bruijn, Expansion of human mesenchymal stromal cells on microcarriers: growth and metabolism, J Tissue Eng Regen Med 4 (2) (2010) 131–140, https://doi.org/10.1002/term.224.
[45] V.V. Hiew, S.F.B. Simat, P.L. Teoh, The advancement of biomaterials in regulating stem cell fate, Stem Cell Rev Rep 14 (1) (2018) 43–57, https://doi.org/10.1007/s12015-017-9764-y.
[46] X. Chen, J. Chen, D. Xu, S. Zhao, H. Song, Y. Peng, Effects of Osteoglycin (OGN) on treating senile osteoporosis by regulating MSCs, BMC Muscoskel. Disord. 18 (1) (2017) 423, https://doi.org/10.1186/s12891-017-1779-7.
[47] K.-i. Tanaka, E. Matsumoto, Y. Higashimaki, T. Katagiri, T. Sugimoto, S. Seino, H. Kaji, Role of osteoglycin in the linkage between muscle and bone, J. Biol. Chem. 287 (15) (2012) 11616–11628, https://doi.org/10.1074/jbc.M111.292193.
[48] N. Zhou, Q. Li, X. Lin, N. Hu, J.-Y. Liao, L.-B. Lin, C. Zhao, Z.-M. Hu, X. Liang, W. Xu, H. Chen, W. Huang, BMP2 induces chondrogenic differentiation, osteogenic differentiation and endochondral ossification in stem cells, Cell Tissue Res. 366 (1) (2016) 101–111, https://doi.org/10.1007/s00441-016-2403-0.
[49] I. Sekiya, H. Katano, N. Ozeki, Characteristics of MSCs in synovial fluid and mode of action of intra-articular injections of synovial MSCs in knee osteoarthritis, Int. J. Mol. Sci. 22 (6) (2021), https://doi.org/10.3390/ijms22062838.
[50] Q.A. Rafiq, Toward a scalable and consistent manufacturing process for the production of human MSCs, Cell and Gene Therapy Insights 2 (1) (2016) 127–140. %@ 2059-7800.
[51] V. Jossen, C. van den Bos, R. Eibl, D. Eibl, Manufacturing human mesenchymal stem cells at clinical scale: process and regulatory challenges, Appl. Microbiol. Biotechnol. 102 (9) (2018) 3981–3994, https://doi.org/10.1007/s00253-018-8912-x.
[52] A.A. Sherstneva, T.S. Demina, A.P.F. Monteiro, T.A. Akopova, C. Grandfils, A.B. Ilangala, Biodegradable microparticles for regenerative medicine: a state of the art and trends to clinical application, Polymers (Basel) 14 (7) (2022) 1314–4360. %@ 2073.
[53] E.X. Ng, M. Wang, S.H. Neo, C.A. Tee, C.-H. Chen, K.J. Van Vliet, Dissolvable gelatin-based microcarriers generated through droplet microfluidics for expansion and culture of mesenchymal stromal cells, Biotechnol. J. 16 (3) (2021), e2000048, https://doi.org/10.1002/biot.202000048.
[54] X. Yan, K. Zhang, Y. Yang, D. Deng, C. Lyu, H. Xu, W. Liu, Y. Du, Dispersible and dissolvable porous microcarrier tablets enable efficient large-scale human mesenchymal stem cell expansion, Tissue Eng. C Methods 26 (5) (2020) 263–275, https://doi.org/10.1089/ten.TEC.2020.0039.